Controllable Photoelectric Properties of Carbon Dots and Their Application in Organic Solar Cells

Wen-Sheng Zhao[a,c], Xin-Xin Li[a], Han Zha[b], Yong-Zhen Yang[a*], Ling-Peng Yan[a,b,c*], Qun Luo[c], Xu-Guang Liu[a,b], Hua Wang[a,d], Chang-Qi Ma[c], and Bing-She Xu[a]

[a] *Key Laboratory of Interface Science and Engineering in Advanced Materials, Ministry of Education, Taiyuan University of Technology, Taiyuan 030024, China*
[b] *College of Materials Science and Engineering, Taiyuan University of Technology, Taiyuan 030024, China*
[c] *Printed Electronics Research Center, Suzhou Institute of Nano-Tech and Nano-Bionics, Chinese Academy of Sciences (CAS), Suzhou 215123, China*
[d] *Ministry of Education and College of Textile Engineering, Taiyuan University of Technology, Jinzhong 030600, China*

Abstract Organic solar cells are a current research hotspot in the energy field because of their advantages of lightness, translucency, roll to roll printing and building integration. With the rapid development of small molecule acceptor materials with high-performance, the efficiency of organic solar cells has been greatly improved. Further improving the efficiency and stability of device and reducing the cost of active layer materials will contribute to the industrial development of organic solar cells. As a novel type of carbon nanomaterials, carbon dots gradually show great application potential in the field of organic solar cells due to their advantages of low preparation cost, non-toxic and excellent photoelectric performance. Firstly, the synthesis and classification of carbon dots are briefly introduced. Secondly, the photoelectric properties of carbon dots and their adjusting, including adjustable surface energy level structure, good film-forming performance and up/down conversion characteristics are summarized. Thirdly, based on these intrinsic properties, the feasibility and advantages of carbon dots used in organic solar cells are discussed. Fourthly, the application progress of carbon dots in the active layer, hole transport layer, electron transport layer, interface modification layer and down-conversion materials of organic solar cells is also reviewed. Finally, the application progress of carbon dots in organic solar cells are prospected. Several further research directions, including in-depth exploration of the controllable preparation of carbon dots and their application in the fields of interface layer and up/down conversion for improving efficiency and stability of device are pointed out.

Keywords Organic solar cells; Carbon dots; Interface layer; Power conversion efficiency; Stability

INTRODUCTION

With the depletion of ore energy and the increasing environmental problems, the demand for renewable and clean energy is particularly urgent. The conversion of solar energy into electricity offers the possibility of sustainable development for mankind. Silicon-based cells, perovskite solar cells, and organic solar cells (OSCs) are all devices that convert solar energy into electrical energy. Among them, OSCs stand out with many unique advantages, such as non-toxic, lightweight, flexible, translucent, and roll-to-roll processing compatible, showing great promise for commercial applications.[1,2] Although OSCs have irreplaceable advantages over other new generation cells, their practical implementation still faces great challenges. Their low photoelectric conversion efficiency and poor stability are important bottlenecks to their development.[3,4] The efficiency and stability of OSCs depend on many factors, such as the structure, composition and contact of functional layers.[5,6]

Usually, researchers mainly improve the performance of solar cells through structural design and morphology control of active layer materials,[7,8] interface layer material modification or replacement.[9]

As a nanomaterial with stable physical and chemical properties and excellent electrical properties, carbon nanomaterials, such as graphene,[10] carbon nanotubes[11] and fullerenes,[12] have been widely used as transparent electrodes,[13] charge transport layers,[14] interface modification layers[15] and active layer materials[16] in OSCs. As a novel type of carbon nanomaterials developed in recent years, carbon dots (CDs), which are a kind of zero-dimensional spherical nanomaterials with diameters less than 10 nm, mainly are composed of carbon, hydrogen, nitrogen and oxygen, with a large number of carboxyl, hydroxyl and amino groups on the surface, mainly hybridized by sp^2 carbon hybridization.[17,18] They gradually show great potential for application in organic solar cell field because of their advantages, including tunable surface state, excellent photovoltaic properties, simple and green preparation, and so on.[19,20] Currently, CDs have been used in OSCs for active layer, interfacial layer and optical down-conversion materials. In this paper, we will summar-

* Corresponding authors, E-mail: yyztyut@126.com (Y.Y.Z.)
 E-mail: yanlingpeng@tyut.edu.cn (L.P.Y)

ize the progress of CDs in the field of OSCs from three aspects: synthesis and classification of CDs, photovoltaic properties and their applications in OSCs, and an outlook on their subsequent research and applications.

SYNTHESIS AND CLASSIFICATION OF CDS

Synthesis

The main synthesis methods of CDs can be divided into top-down method and bottom-up method. The top-down method refers to the physical or chemical method to peel off the nano-carbon materials from the large-sized carbon skeleton (such as carbon target). This method mainly uses laser ablation,[21] arc discharge,[22] electrochemical oxidation[23] and other methods to prepare CDs from large-sized carbon-based materials. For example, CDs can be synthesized from graphene, carbon nanotubes, and biomass[24] by the top-down method. Biomass, such as leaves, fruits, vegetables, can be as a dominant carbon source for the top-down synthesis of CDs because of their unique advantages, including wide selection of materials and low price.[25,26] The bottom-up method refers to the preparation of CDs from some organic molecules as precursors through a series of chemical reactions, which are mainly used to synthesize CDs by carbonization of small molecules (such as citric acid and ethylenediamine[27]) using solvent thermal method/hydrothermal method,[28] microwave synthesis method,[29] combustion/pyrolysis method,[30] and so on. In general, this method requires small organic molecules as precursors under controlled conditions, and these small molecules generally include unsaturated double bonds and reactive sites (functional groups).[31,32] The formation of CDs usually requires high temperature and pressure to coordinate the polymerization and carbonization of small molecules to form CDs, which have good biocompatibility and solvent dispersibility because they can carry the same functional groups as the raw material on their surface.[33] For example, Li *et al*. synthesized CDs with good biocompatibility for promising biomedical applications using citric acid and urea at 160 °C under high pressure.[34] The top-down method is limited by the disadvantages, such as uncontrollable reaction results and low fluorescence quantum yields of the products. In the bottom-up process, microwave synthesis and solvothermal/hydrothermal methods are widely used due to the advantages of high fluorescence quantum yield, high light transmission, low equipment requirements, simple reaction conditions, low cost and environmental friendliness of the products.

Classification

The CDs synthesized from different raw materials and reaction conditions have different structures and properties. CDs can be subdivided into graphitized CDs (GQDs), carbon quantum dots (CQDs), and polymer CDs (PDs).[35] In general, GQDs have a typical carbon lattice structure with different chemical groups bonded to their edges, also known as graphene quantum dots. CQDs do not have an obvious lattice structure, but their edges are still bonded to different chemical groups, also known as carbon nanodots. PDs are non-conjugated polymers or small molecules formed by polymerization, cross-linking, dehydration and carbonization processes to form cross-linked flexible aggregates, whose surface with a large number of polymer chains, also known as carbonized polymer dots.[35]

PHOTOELECTRIC PROPERTIES OF CDS

Optical Absorption

CDs have strong absorption in the ultraviolet-visible (UV-Vis) region (200–400 nm) and their optical absorption can extend to the near-infrared region.[36,37] Yang *et al*.[27] prepared blue-emitting CQDs by hydrothermal method using citric acid and ethylenediamine as carbon sources (Fig. 1a), which had strong optical absorption broad peaks at 250 and 340 nm, corresponding to $\pi\rightarrow\pi^*$ transition of C=C bond and $n\rightarrow\pi^*$ transition of C=O/C=N bond, respectively. In addition, Radek *et al*.[38] prepared a series of red-emitting CQDs using citric acid and urea, which not only had the typical C=C characteristic absorption peaks (250 and 340 nm), but their absorption bands extended to the infrared region, some of them could reach 400–600 nm and even 600–800 nm (Fig. 1b), which is attributed to the presence of aromatic ring structures in CQDs. Tang *et al*.[39] used glucose and ammonia as raw materials to prepare N-doped CQDs (N-CQDs) using microwave-assisted thermal method, the prepared CQDs showed obvious optical absorption in the deep ultraviolet to near infrared region (200–900 nm) (Fig. 1c). It can be seen that the controlled synthesis of CDs with specific absorption spectral range can be achieved by modulating the type of synthetic raw materials and reaction conditions. Generally, CDs synthesized using carbon source rich in C=O/C=C groups will exhibit strong absorption in the ultraviolet region,[40,41] while synthesized using carbon source containing aromatic ring structures or heteroatoms such as sulfur or nitrogen will have long-wave absorption.[38] Therefore, when CDs are applied to OSCs, CDs has optical absorption in the near infrared region, which can be adjusted to broaden the optical absorption range of the active layer of OSCs. Moreover, CDs as the interface layer can block ultraviolet light to avoid its damage to the active layer material.

Energy Level Tunability

Numerous researches have shown that the band gap of CDs is influenced by the carbon core size,[42] surface state[43] and concentration.[44] The surfaces of CDs are rich in a large number of —OH, —COOH, —NH₂ and other groups (Fig. 2). Their carbon core size, surface groups and solution concentration can be regulated by controlling the reaction materials and reaction conditions, and finally their energy level can be adjusted.

In most cases, the band gap of CDs is decreased with the increased size.[45] Li *et al*.[45] sliced graphite into 1.2–3.8 nm GQDs. By testing the photoluminescent (PL) spectra of GQDs with different sizes, they found that when the size increases, the emission peak red shifted, indicating that the band gap of GQDs decreased. They further obtained the same conclusion by simulating the energy level difference between the lowest unoccupied molecular orbital (LUMO) and the highest occupied molecular orbital (HOMO) of GQDs. Tian *et al*.[46] found that increasing the amount of C—OH and C—N groups on the surface of CQDs could reduce the band gap bending degree and accelerate the recombination of electron-hole pairs. The introduction of C—Cl group on the surface of CQDs could form a micro electric field with C—O group to promote the
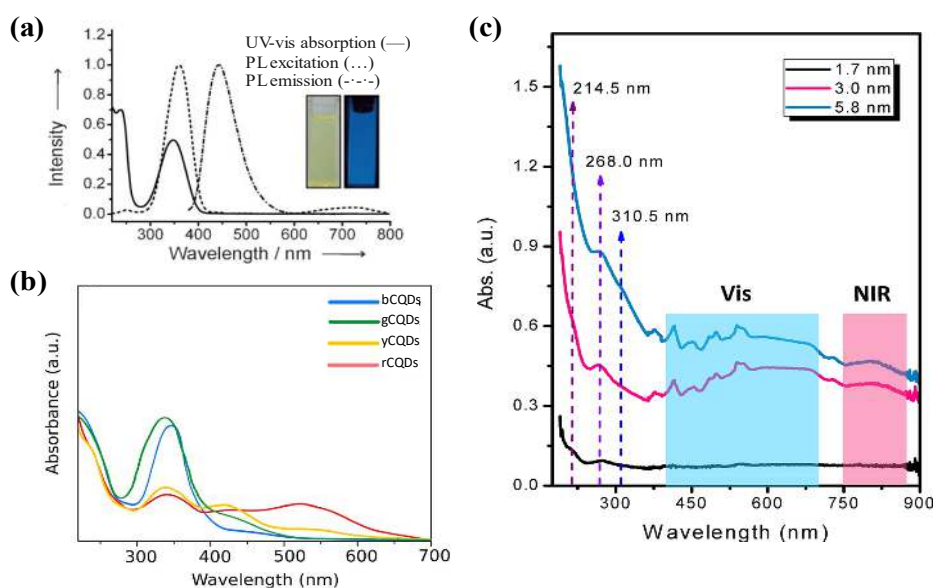
Fig. 1 (a) UV-Vis absorption spectra of typical CQDs. (Reproduced with permission from Ref. [27]; Copyright (2013) Wiley); (b) UV-Vis absorption spectra of CQDs with red light absorption (The different curves represent CQDs that emit different colors (blue, green, yellow, red)). (Reproduced with permission from Ref. [38]; Copyright (2017) American Chemical Society); (c) UV-Vis absorption spectra of CQDs with deep ultraviolet-near infrared light absorption (the different curves represent different sizes of CQDs). (Reproduced with permission from Ref. [39]; Copyright (2014) American Chemical Society).
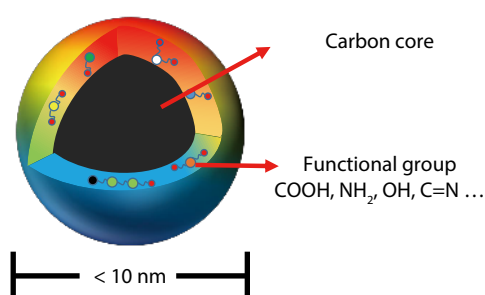

Fig. 2 Schematic diagram of the carbon core and functional groups of typical CDs.

separation of electrons and holes, so as to realize the tunable energy level of CQDs. Su *et al.*[44] prepared CQDs by pyrolysis using citric acid and thiourea, which not only had fluorescence emission-dependent properties but also change the energy gap width of CQDs by adjusting the raw material concentration. As shown in Fig. 3, the band gap decreases from 2.18 eV to 1.56 eV when the concentration of CQDs was increased from 0.002 mg/mL to 1.0 mg/mL, and they speculated that this might be due to the aggregation of CQDs caused by the increase in their concentration, which in turn affects their surface states to change the band gap. In addition, Ran *et al.*[47] prepared CQDs with an optical band gap ranging from 3.1 eV to 4.2 eV by redox method to tune the surface structure of CQDs for adjusting the mutual jump between the single and triplet excitons. The tunable energy level of CDs can be used in the functional layer of OSCs to adjust the energy level of each layer, and finally reduce the energy loss and improve the photoelectric conversion efficiency of the cells.
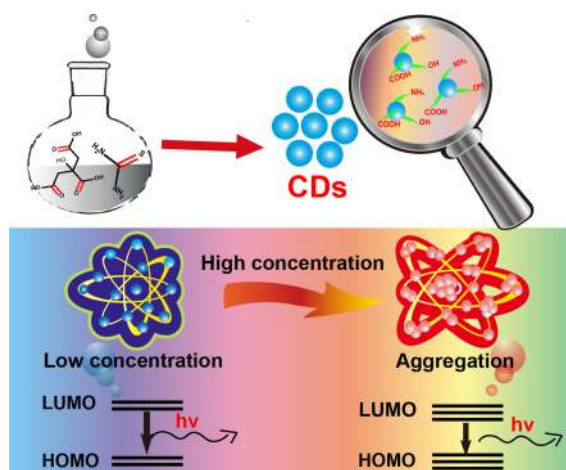

Fig. 3 Schematic diagram of CQDs synthesis and their energy level adjustability by adjusting concentration. (Reproduced with permission from Ref. [44]; Copyright (2020) Elsevier).

Up/Down-conversion Fluorescence Properties

CDs absorb short-wavelength photons to the excited state, and emit long-wavelength light when photons return to the ground state, a phenomenon known as the down-conversion fluorescence property of CDs, which follows the Stokes effect, *i.e.*, the emission wavelength is larger than the excitation wavelength. The redshift of the fluorescence spectrum emission wavelength compared to the absorption spectrum is called the Stokes shift. The larger the Stokes shift, the larger the difference between the emission wavelength and the absorption wavelength. In OSCs, it is expected the Stokes shift is as large as possible, because too small Stokes shift can produce internal conversion, which will reduce the photoelectric

conversion efficiency of OSCs, and the larger Stokes shift is beneficial for converting the ultraviolet absorption part of the solar light into visible light or even near-infrared light, which improves the spectral response ability of the device in the ultraviolet band and increases the photoelectric conversion efficiency of OSCs.[15,48] It has been well reported that CDs can emit longer wavelengths of light under UV excitation with significant Stokes shifts,[49–52] and they exhibit fluorescence excitation wavelength dependence[49,50] or independence,[51,52] respectively. Most researchers suggest that the fluorescence excitation wavelength dependence of CDs is related to the quantum size effect of carbon core, surface states, and molecular fluorescence induced by large π-bonds. For example, Zhang et al.[53] prepared CQDs from citric acid and cysteine by hydrothermal method to emit blue light with fluorescence excitation wavelength dependence and fluorescence quantum yield of 31%.The wavelength independence of fluorescence emission of CDs also were reported. For example, Lu et al.[52] synthesized CQDs from dopamine and o-phenylenediamine by hydrothermal method at 200 °C with significant excitation wavelength independence, as evidenced by their emission center of 710 nm under white light excitation, and these CQDs also had near-infrared luminescence properties and possess two-photon fluorescence properties. CDs with down-conversion fluorescence properties can convert ultraviolet light into visible light that can be absorbed by the active layer of OSCs. On the one hand, it broadens the spectral absorption of OSCs, and on the other hand, it prevents ultraviolet light from damaging the active layer, resulting in enhanced efficiency and stability of OSCs.

In recent years, the unique up-conversion luminescence mechanism possessed by CDs was successively reported.[52,54–56] The essence of up-conversion luminescence is the anti-Stokes effect, which is widely believed to be caused by the successive absorption of two or more low-energy photons leading to high-energy luminescence.[57] According to Molaei et al.,[58] CQDs had strong visible emission under the excitation of argon ion laser (458 nm) and femtosecond pulsed laser (800 nm), and the quadratic relationship between excitation laser power and luminescence intensity confirms that the visible luminescence was caused by the excitation of two near-infrared photons. For example, He et al.[59] prepared CQDs by hydrothermal method with citric acid and ethanolamine at 180 °C and emitted blue light under red light excitation, which confirmed that the up-conversion performance of CQDs is due to two-photon excitation.

More interestingly, Jia et al.[54] prepared CQDs by direct heating of ascorbic acid at 90 °C with both down-conversion and excellent up-conversion properties. CQDs emitted blue light under UV excitation and green light at 540 nm under near-infrared (NIR) excitation at 800–1000 nm, which may be due to the absorption of multiple photons by CQDs. Although most researchers believe that the up-conversion properties of CQDs should be attributed to multiphoton processes,[60,61] Shen et al.[55] speculated that the up-conversion of CQDs cannot only be explained by multiphoton processes because the emission and excitation have a constant energy difference corresponding to the energy difference between π and σ orbitals (1.1 eV). They suggested that the π-electron

(in the intermediate energy level) is excited by a low-energy photon to the LUMO and thereafter relaxed to the σ-orbitals of HOMO, leading to the emission of a shorter wavelength photon. Fig. 4 is the schematic diagram of the electron leap process of CQDs. Figs. 4(a) and 4(b) show the fluorescence emission at excitation wavelengths for CQDs with large and small sizes without anti-Stokes shift property, respectively. The band gap of CQDs (difference between LUMO and HOMO) depends on the size of CQDs, and the band gap becomes smaller as the size of CQDs increases. And the up-conversion fluorescence performance of CQDs with anti-Stokes shift property is shown in Figs. 4(c) and 4(d). Shen et al. suggested that when a beam of low-energy photons excites electrons in a π orbital (Figs. 4c and 4d), the π electrons transition to a high-energy state (LUMO energy level) and then to a low-energy state. Thus, when the electrons jump back to the σ orbital, up-conversion fluorescence is emitted. Although the electrons in the σ orbital can also leap, it can only emit normal PL (Figs. 4a and 4b), which can explain a phenomenon that the excited and emitted light is a constant energy difference.
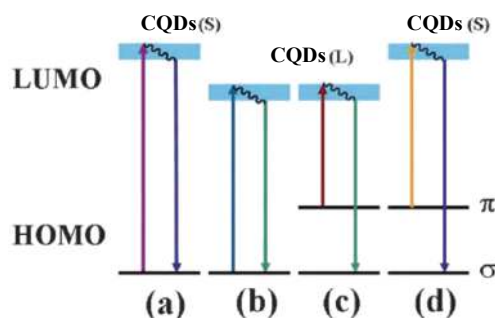

Fig. 4 Schematic diagrams of various typical electronic transition processes of CQDs. (a) Normal PL mechanism in small-size and (b) large-size CQDs; up-conversion PL mechanism in (c) large-size and (d) small-size CQDs. (Reproduced with permission from Ref. [55]; Copyright (2011) the Royal Society of Chemistry).

The unique up/down-conversion fluorescence properties of CDs can be used to broaden the light absorption range of OSCs, thus enhancing the photogenerated current and ultimately improving the device performance. According to the theoretical calculations by Shockley-Queisser et al.,[62] the theoretical photoelectric conversion limit efficiency of solar cells is 33.7%, which is due to the energy loss in the photoelectric conversion process, as shown in Fig. 5.[63] Among them, the lattice thermal vibration and transmission loss (①, ②) caused by spectral mismatch account for more than 70% of the total loss, which is the main source of energy loss. The absorption spectra of the active layer materials of most fullerene-based OSCs are in the visible region, and the light conversion rate is almost 0 below 400 nm and above 800 nm. Even the recently developed non-fullerene acceptor materials have absorption spectra only up to about 1000 nm. The spectral mismatch has limited the further improvement in photoelectric conversion efficiency of OSCs. Therefore, if the up/down-conversion fluorescence property of CDs can be effectively utilized, the sunlight in the IR/UV region will be utilized to increase the number of absorbed photons in the active layer and gener-
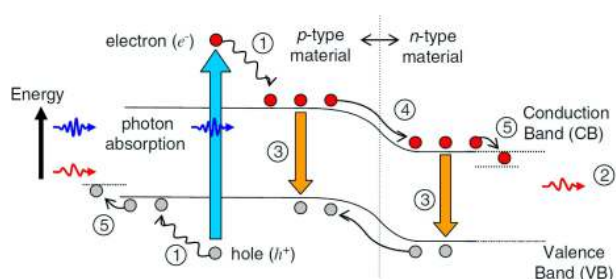
Fig. 5 Energy loss process of single junction solar cell: ① lattice heat loss ② transmission loss ③composite loss ④ heterojunction loss ⑤ contact voltage loss. (Reproduced with permission from Ref. [63]; Copyright (2006) Elsevier).

ate more excitons, finally improve the photoelectric conversion efficiency of the cell. At present, the down-conversion fluorescence property of CDs has been initially tried in OSCs, the details as seen in **Section 3.2.4**,[64] but the up-conversion property has rarely been reported.

Solution Processing Properties of CDs

Most of the CDs with rich functional groups are mainly synthesized in bulk by microwave and solvothermal methods, and have excellent dispersion properties in solvents. It is worth emphasizing that in order to achieve good dispersion properties of CDs in the target solvent, the surface pro/hydrophobic properties of CDs need be controlled by modulating the reaction solvent, leading to their good solution processing properties and excellent film-forming properties. The future development trend of OSCs is bound to be large-scale printing by solution method.[65] The solution dispersibility and stability of CDs are positively correlated with the film-forming performance, *i.e.*, the stronger the solvent dispersion and stability, the higher the formed film quality. Mao *et al.*[66] successfully prepared CQDs fluorescent membrane sensors by molecular self-assembly method and suggested the preparation conditions including concentration, solvent and assembly temperature have a great influence on the film-forming performance of CQDs. The results showed that CDs fluorescent membrane sensors with high fluorescence intensity and uniform and dense membrane coverage was prepared when the CQDs content was 10%, the solvent was trichloromethane and the assembly temperature was 50 °C. The large number of functional groups on the surface of CDs gives them the ability to control their concentration, disperse the solvent type and finally achieve guided film formation. Generally, by controlling the number of hydrophilic and hydrophobic groups on the surface of the CDs, the dispersion performance in water or organic solvents can be respectively controlled, and finally high-quality film-forming performance control can be achieved.

In conclusion, CDs have excellent optical properties, suitably matched and tunable energy level structures, up/down-conversion characteristics and good solution processing properties, which are conducive to improving the performance of OSCs and promoting their commercialization.

APPLICATION OF CARBON DOTS IN ORGANIC SOLAR CELLS

The main structures of single-junction OSCs are divided into conventional and inverted structures,[67] where the latter has higher stability compared to the former.[68] In both types of structures, in addition to the cathode and anode electrodes that collect electrons and holes, they include the electron transport layer (ETL) and the hole transport layer (HTL) that transport electrons and holes, respectively, and the active layer that generates photogenerated charges. At present, CDs have been gradually applied in the field of OSCs for excellent performance, and the current main used as active layer materials, interfacial layer materials and down-conversion materials for OSCs.

Active Layer

The active layer is the most important part of an organic solar cell. Theoretically, the active layer material determines the limit of the photoelectric conversion efficiency of OSCs. The active layers in OSCs include donors and acceptors, which usually exist as bulk heterojunctions with interpenetrating network structure. In the running process, the donors and acceptors absorb photons and generate excitons, which are separated at the donor/acceptor interface to generate charges. Then the charges are collected by the electrodes, resulting in potential difference and current.

CDs are used in the active layer of OSCs due to their excellent photovoltaic properties. Table 1 summarizes the device performance of CDs used as active layers for OSCs in recent years. It can be seen that CDs alone as acceptors is not comparable to fullerene-based acceptors, however, they can further enhance the device performance of OSCs when used as active layer doping materials. For example, Kwon *et al.*[69] prepared CQDs with tunable particle size by a soft template method. Using them as acceptors, an organic solar cell with ITO/PEDOT:PSS/P3HT:CQDs/Al structure with an efficiency of 0.23% was prepared. Sharma *et al.*[70] prepared three acceptor materials: CQDs, ZnO-decorated graphene (Zn@G) and carbon quantum dots modified ZnO (Zn@CQDs), which were as acceptor, respectively, and PFO-DBT as donor to prepare OSCs (Table 1). It can be seen that the introduction of CQDs largely improved the short-circuit current (J_{sc}) and open-circuit voltage (V_{oc}) of the cells, in which the cell performance was significantly improved when Zn@CQDs are used as the acceptor, which may be due to the fact that Zn@CQDs were more likely to form good contact with the donor materials (generally polymers).

Further, researchers found that doping CDs in the active layer is an effective and convenient method to enhance the performance of OSCs. Zhang *et al.*[73] prepared inverted OSCs with the structure of ITO/PEI/P3HT:ICBA:CQDs/MoO$_3$/Ag by doping CQDs into the active layer of P3HT:ICBA, and the results showed that the device efficiency was improved by 43.20% (from 4.12% to 5.90%) when the CQDs doping concentration was only 3 wt%, which was mainly because the uniform dispersion of CQDs in the active layer could improve the charge carrier transport and reduce charge complexation, meanwhile, the introduction of CQDs could increase the optical path scattering to increases the light absorption of the device. by doping carbon nitride quantum dots (C_3N_4) into the active layer, Chen *et al.*[64] prepared OSCs with P3HT, PB-DTTT-C, PTB7-Th as the donor and PC$_{71}$BM as the acceptor materials. The efficiency of the devices was improved by 17.5%, 11.6% and 11.8%, respectively, compared with the ref-

Table 1 Summary of photovoltaic parameters of OSCs using CDs as acceptor or doped materials.(The photovoltaic parameters are compared to those measured for a reference cell (values in parentheses).)

Device structure	J_{sc}(mA/cm^2)	V_{oc}(V)	FF	PCE(%)	Refs.
ITO/PEDOT:PSS/P3HT:CQDs/Al	0.29	1.59	0.49	0.23	[69]
ITO/PEDOT:PSS/PFO-DBT:CQDs/Al	12.00	0.88	0.26	2.75	[70]
ITO/PEDOT:PSS/PFO-DBT:Z@G/Al	12.50	0.76	0.32	3.04	[70]
ITO/PEDOT:PSS/PFO-DBT:Z@CQDs/Al	14.80	0.82	0.32	3.88	[70]
ITO/PEDOT:PSS/PTB7:PC$_{71}$BM:GQDs/TiO$_x$/Al	15.20	0.74	0.68	7.60	[10]
(ITO/PEDOT:PSS/PTB7:PC$_{71}$BM/TiO$_x$/Al)	(15.20)	(0.74)	(0.60)	(6.70)	[10]
ITO/PEIE/P3HT:PC$_{60}$BM:CQDs/MoO$_3$/Al	8.00	0.65	0.67	3.48	[71]
(ITO/PEIE/P3HT:PC$_{60}$BM/MoO$_3$/Al)	(6.90)	(0.64)	(0.62)	(2.74)	[71]
ITO/TiO$_2$/PCDTBT:PCBM:CQDs/MoO$_3$/Ag	13.61	0.87	0.60	7.05	[72]
(ITO/TiO$_2$/PCDTBT:PCBM/MoO$_3$/Ag)	(12.86)	(0.87)	(0.49)	(5.50)	[72]
ITO/PEI/P3HT:ICBA:CQDs/MoO$_3$/Ag	11.31	0.85	0.61	5.90	[73]
(ITO/PEI/P3HT:ICBA/MoO$_3$/Ag)	(8.93)	(0.84)	(0.55)	(4.12)	[73]
ITO/ZnO/C$_3$N$_4$:P3HT:PC$_{61}$BM/MoO$_3$/Ag	11.44	0.61	0.60	4.56	
(ITO/ZnO/P3HT:PC$_{61}$BM/MoO$_3$/Ag)	(10.09)	(0.60)	(0.60)	(3.80)	
ITO/ZnO/C$_3$N$_4$:PBDTTT-C:PC$_{71}$BM/MoO$_3$/Ag	15.90	0.70	0.57	6.62	
(ITO/ZnO/PBDTTT-C:PC$_{71}$BM/MoO$_3$/Ag)	(14.30)	(0.72)	(0.55)	(5.83)	[64]
ITO/ZnO/C$_3$N$_4$:PTB7-Th:PC$_{71}$BM/MoO$_3$/Ag	16.74	0.78	0.70	9.20	
(ITO/ZnO/PTB7-Th:PC$_{71}$BM/MoO$_3$/Ag)	(15.91)	(0.77)	(0.67)	(8.39)	[64]
ITO/ZnO/P3HT:CQDs/MoO$_3$/Al	0.77	0.62	0.60	0.29	[74]
(ITO/ZnO/P3HT/MoO$_3$/Al)	(0.27)	(0.55)	(0.52)	(0.08)	[74]

erence devices, due to the improved contact between the active layer and hole transport layer by doping C$_3$N$_4$ and the down-conversion performance of C$_3$N$_4$.

Interface Layer

In OSCs, the interfacial layer includes ETL and HTL, which are responsible for transporting electrons and holes generated by the active layer to the cathode and anode, respectively, finally generating a potential difference. The low efficiency and poor stability of OSCs, to a large extent, originate from the instability of the interfacial layer materials.[75] For example, PEDOT:PSS is well-matched with most anode materials and active layer materials in terms of work function, but it is very sensitive to water and oxygen, which results in the poor stability of OSCs. Furthermore, the materials used as the interface layers require the high light transmission, otherwise it will reduce the absorption of the active layer to sunlight. Therefore, CDs as interface layer materials have a large potential due to their high stability, adjustable work function, and high light transmission.[15] In addition, some researchers have developed the composite interface layers by combining CDs with conventional interface layers to improve performance of OSCs.[76]

Electron transport layer

For the ETL materials, the low work function and high stability are the most basic requirements, and their low sensitivity to thickness, and stronger light transmission is the priority for the preparation of future high-efficiency OSCs. The modulation of the surface functional groups on CDs, which makes energy level structure more compatible with other layers, is a common method to enhance the performance of OSCs. The performance of single electron transport layers constructed by CDs for OSCs is comparable to or even better than those of ordinary ETLs. For example, Xu et al.[77] deposited GQDs with ammonium iodide (GQDs-NI) on the surface of Ag, which reduced the work function from 4.8 eV to 3.8 eV, and the work function of Al electrode after GQDs-NI deposition is even reduced to 3.6 eV. The lower cathode work function was conducive to the formation of ohmic contact between the active layer and cathode, which can reduce the energy loss in the process. Ding et al.[78] used the GQDs-TMA prepared by grafting tetramethylammonium (TMA) with CQDs for the ETL of PTB7-Th:PC$_{71}$BM-based OSCs (as shown in Fig. 6a). The device efficiency reached 7.01%, while the other devices using Ca, ZnO, LiF were under 6.5% at the same conditions, which was attributed to the fact that GQDs-TMA can effectively reduce the cathode work function (Figs. 6b and 6c) to induce the formation of ohmic contact between the Al electrode and the active layer, finally reducing energy loss.

Our group has also explored the application of CDs in the ETL of OSCs. For example, Yan et al.[79] used chemical vapor deposition to synthesize CQDs with an average diameter of 3.5 nm and hydrophobic —CH$_3$ groups on their surface, which exhibited good dispersion in organic solvents. Using these CQDs instead of LiF and Ca as the ETL in OSCs, the results showed that the efficiency of CQDs-based OSCs is comparable to that of LiF devices, but the thermal stability is greatly improved.

From the above-mentioned examples, it can be concluded that CDs have great potential for application in the field of ETL of high-performance OSCs, which can replace unstable materials (e.g., LiF, Ca, etc.) and be used as ETL materials alone to compensate for the disadvantages of other materials.

Hole transport layer

CDs can be used not only as ETL, but also as an ideal HTL material for high-performance OSCs because of their good electrical conductivity, tunable work function and dispersion. Table 2 summarizes the device performance parameters of CDs used as ETL and HTL for OSCs in recent years. As reported by Li et al.,[80] the efficiency of OSCs based on CQDs as the HTL and P3HT:PC$_{61}$BM as the active layer reached 3.51%, which was comparable to that of PEDOT:PSS. And the device maintained 45% of the initial efficiency after exposure to air for more than 8000 min, but the efficiency of PEDOT:PSS-based devices under the same conditions decayed to 0 (Fig. 6d). In addition, CQDs-based cells exhibited low thickness sensitivity, and the efficiency of CQDs-based devices was almost unaffected when the CQDs film thickness increases to 7 nm (Fig. 6e). Ding et al.[81] used surface carboxyl-rich CQDs as HTL to prepare OSCs with PTB7 and PCDTBT as donor materials and PC$_{71}$BM as acceptor
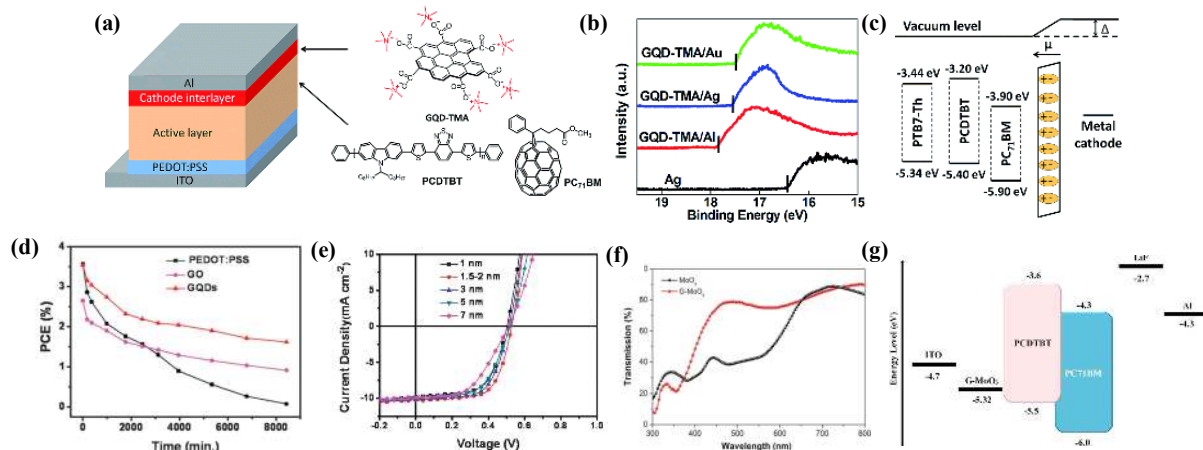
Fig. 6 (a) Device structure of OSCs based on GQD-TMA as ETL and structural formula of GQD-TMA, PCDTBT, PCBM; (b) Ultraviolet photoelectron spectroscopy of GQD-TMA/Au, GQD-TMA/Al and GQD-TMA/Ag; (c) Work function schematic diagrams of energy levels. (Reproduced with permission from Ref. [78]; Copyright (2016) the Royal Society of Chemistry); (d) Degradation curves of OSCs based on PEDOT:PSS and CQDs as the hole transport layer and (e) current-voltage curves of OSCs with different thicknesses of CQDs. (Reproduced with permission from Ref. [80]; Copyright (2013) the Royal Society of Chemistry). (f) Optical transmittance curves of G-MoO$_3$ and MoO$_3$; (g) Schematic diagram of the work function of each layer of the organic solar cell. (Reproduced with permission from Ref. [85]; Copyright (2019) Elsevier).

Table 2 Summary of photovoltaic parameters of OSCs with CDs as electron transport layer or hole transport layer. (The photovoltaic parameters are compared to those measured for a reference cell (values in parentheses).)

	Device structure	J_{sc}(mA/cm^2)	V_{oc}(V)	FF	PCE(%)	Refs.
ETL	ITO/PEDOT:PSS/PCDTBT:PC$_{71}$BM/GQD-Ni/Al(ITO/PEDOT:PSS/PCDTBT:PC$_{71}$BM/Al)	10.98(10.31)	0.93(0.86)	0.73(0.61)	7.45(5.41)	[77]
	ITO/PEDOT:PSS/PTB7-Th:PCBM/GQD-TMA/Al(ITO/PEDOT:PSS/PTB7-Th:PCBM/Al)	17.39(17.28)	0.76(0.74)	0.67(0.59)	8.85(7.54)	[78]
	ITO/PEDOT:PSS/PTB7-Th:PC$_{71}$BM/GQDs/Al(ITO/PEDOT:PSS/PTB7-Th:PC$_{71}$BM/Al)	9.49(8.76)	0.63(0.59)	0.51(0.31)	3.05(1.60)	[79]
	ITO/PEDOT:PSS/DR3TBDTT:PC$_{71}$BM/CQDs/Al(ITO/PEDOT:PSS/DR3TBDTT:PC$_{71}$BM/Al)	13.32(12.88)	0.90(0.90)	0.64(0.61)	7.67(7.07)	[82]
HTL	ITO/GQDs/P3HT:PC$_{71}$BM/LiF/Al(ITO/P3HT:PC$_{71}$BM/LiF/Al)	10.20(8.15)	0.52(0.44)	0.66(0.56)	3.51(2.02)	[80]
	ITO/GQDs/PTB7:PC$_{71}$BM/LiF/Al(ITO/PTB7:PC$_{71}$BM/LiF/Al)	15.20(13.51)	0.75(0.64)	0.69(0.61)	7.91(5.27)	[81]
	ITO/GQDs/PCDTBT:PC$_{71}$BM/LiF/Al(ITO/PTB7:PC$_{71}$BM/LiF/Al)	10.65(9.92)	0.89(0.52)	0.67(0.59)	6.30(3.03)	

material, respectively. The device efficiencies (7.91%, 6.30%) were higher than those of the PEDOT:PSS materials (7.46%, 6.02%) and the hole-free transport layer materials (5.27 %, 3.03%), which was because the higher work function of the surface carboxyl-rich CQDs can reduce the potential difference with the anode.

Interface modification layer

CDs can be used not only as the active layer and electron/hole transport layer, but also can modify the interface layers, including the electron/hole transport layer, cathode and anode, to adjust the work function for enhancing the device performance of OSCs. Table 3 lists the device performance of CDs modifying electron/hole transport layers in recent years. Because the abundant variety of functional groups on the surface of CDs give them good dispersion in various solvents, they can be mixed with other HTLs such as PEDOT:PSS without severe aggregation. Hasani et al.[83] prepared OSCs by co-doping CQDs with tetra(4-sulfonatophenyl)porphyrin (Fe(III)tetra(4-sulfonatophenyl)porphyrin, FeTSPP) with PEDOT:PSS as the hole transport layer. The device performance was improved from 3.17% to 4.68% and the stability was also significantly improved. The analysis showed that the doping of CQDs with FeTSPP jointly adjusted the work function of PEDOT:PSS to better match the active layer and anode, which enhanced the hole transport

capability. Kim et al.[84] reported a CQDs:PEDOT:PSS composite HTL. They found that the addition of CQDs induced the increase of grain size of PEDOT:PSS, which may be due to the interaction between negatively charged CQDs and positively charged PEDOT, resulting in a significant increase in the current density of the device, and the photoelectric conversion efficiency of the device was increased from 7.52% to 8.17%. In addition, the better results were obtained by compounding CQDs with other conventional HTL materials. Dang et al.[85] prepared G-MoO$_3$ by compounding prepared GQDs with molybdenum oxide as HTL and conventional structured OSCs with device structure of ITO/G-MoO$_3$/PCDTBT:PC$_{71}$BM/LiF/Al. The device efficiency reached 7.07%, while the MoO$_3$-based device efficiency was only 5.72%, which was attributed to the higher optical transmission of G-MoO$_3$ and the improved energy level matching with the anode and active layer. From Fig. 6(f), the optical transmittance of G-MoO$_3$ is significantly stronger than that of MoO$_3$ between 400–600 nm, which is the main band of visible light, suggesting that the use of G-MoO$_3$ HTL is more beneficial for the active layer to absorb more photon. The matching degree of G-MoO$_3$ with ITO and active layer (Fig. 6g) showed that the work function of G-MoO$_3$ (−5.32 eV) matched better with the HOMO (−5.5 eV) of the donor, which was more favorable for the formation of ohmic contact between the active

Table 3 Summary of photovoltaic parameters of OSCs with CDs modified electron transport layer or hole transport layer. (The photovoltaic parameters are compared to those measured for a reference cell (values in parentheses).)

Device structure	J_{sc}(mA/cm^2)	V_{oc}(V)	FF	PCE(%)	Refs.
ITO/G-MoO$_3$/PCDTBT:PC$_{71}$BM/LiF/Al(ITO/MoO$_3$/PCDTBT:PC$_{71}$BM/LiF/Al)	12.83(11.02)	0.86(0.86)	0.64(0.61)	7.07(5.72)	[85]
ITO/ZnO:CQDs/PTB7-Th:PC$_{71}$BM/MoO$_3$/Al(ITO/ZnO/PTB7-Th:PC$_{71}$BM/MoO$_3$/Al)	17.20(16.88)	0.80(0.80)	0.68(0.68)	9.36(9.18)	[76]
ITO/CD@ZnO/PM6:IT-4F/MoO$_3$/Al(ITO/ZnO/PM6:IT-4F/MoO$_3$/Al)	20.75(20.44)	0.83(0.81)	0.71(0.68)	12.23(11.26)	[86]
ITO/CQD@PEI/PTB7:PC$_{71}$BM/MoO$_3$/Ag(ITO/PEI/PTB7:PC$_{71}$BM/MoO$_3$/Ag)	18.37(16.46)	0.73(0.73)	0.71(0.61)	9.52(7.33)	[92]
ITO/ZnO:CQDs/PTB7:PC$_{71}$BM/MoO$_3$/Al(ITO/ZnO/PTB7:PC$_{71}$BM/MoO$_3$/Al)	17.78(16.65)	0.76(0.75)	0.75(0.70)	10.13(8.74)	[93]
ITO/ZnO:CND/PTB7-Th:PC$_{71}$BM/MoO$_3$/Ag(ITO/ZnO/PTB7-Th:PC$_{71}$BM/MoO$_3$/Ag)	17.00(15.60)	0.77(0.79)	0.73(0.68)	9.56(8.38)	[94]
ITO/ZnO:CND/PBDB-T:ITIC/MoO$_3$/Ag(ITO/ZnO/PBDB-T:ITIC/MoO$_3$/Ag)	15.80(15.20)	0.91(0.91)	0.64(0.61)	9.20(8.44)	[94]
ITO/AZO:CQDs/PTB7-Th:PC$_{71}$BM/MoO$_3$/Al(ITO/AZO/PTB7-Th:PC$_{71}$BM/MoO$_3$/Al)	18.12(16.63)	0.80(0.79)	0.71(0.68)	10.29(8.93)	[15]
ITO/AZO:CQDs/PTB7:PC$_{71}$BM/MoO$_3$/Al(ITO/AZO/PTB7:PC$_{71}$BM/MoO$_3$/Al)	17.65(16.19)	0.75(0.73)	0.70(0.67)	9.27(7.92)	[15]
ITO/TiO$_2$:CQD/PCDTBT:PC$_{71}$BM/MoO$_3$/Ag(ITO/TiO$_2$/PCDTBT:PC$_{71}$BM/MoO$_3$/Ag)	15.02(14.58)	0.85(0.85)	0.57(0.55)	7.28(6.82)	[95]
ITO/PEI:CQDs/PTB7-Th:PC$_{71}$BM/MoO$_3$/Ag(ITO/PEI:CQDs/PTB7-Th:PC$_{71}$BM/MoO$_3$/Ag)	17.24(16.43)	0.77(0.77)	0.71(0.67)	9.49(8.56)	[88]

layer and the anode with less energy loss.

CDs can be used not only as HTL modification materials, but also as ETL modification materials. Wang et al.[76] used co-blended mixture of N,S-doped CQDs (N,S-CQDs) and ZnO as the ETL in OSCs, and found the introduction of N,S-CQDs passivated the surface defects of ZnO and suppressed the "light soaking" phenomenon. Zhao et al.[86] prepared amino-containing CQDs by hydrothermal method with citric acid and ethylenediamine, and *in situ* synthesized CQDs@ZnO core-shell dots, which improved the crystallization of ZnO and effectively inhibited the aggregation of ZnO. At the same time, the introduction of CQDs could adjust the work function of ZnO, which made it more compatible with the active layer and cathode, forming a good ohmic contact. The final device performance was improved from 11.26% to 12.23%. Zhang et al.[87] used CQDs modifying ZnO to prepare inverted OSCs with P3HT:PC$_{61}$BM and PTB7:PC$_{71}$BM as active layers, respectively, and the device structures are shown in Fig. 7(a). The results showed that modifying ZnO with CQDs could increase the contact between the active layer and ZnO as well as reduce the exciton recombination, and the final device efficiency was improved. In addition, CQDs can also be applied to multi-junction OSCs. Kang et al.[88] used CQDs to modify the PEI and prepared single- and multi-junction OSCs, respectively, as shown in Figs. 7(c) and 7(d). The device efficiencies reached 9.49% and 12.13%, respectively, with 10.9% and 15.1% performance improvement compared to pure PEI devices. From the impedance plots in Figure 7e and f, the impedance of the organic solar cell was significantly reduced after the doping of CQDs, and had the less compound at the interface.

Interestingly, CDs are also used to modify the electrodes. Li et al.[89] used the prepared onion-like carbon dots (OLCNs) to modify the Ag to prepare OSCs with PTB7:PC$_{71}$BM as the active layer, and the efficiency increased from 7.76% to 9.81%. OLCNs could not only increase the work function of Ag, but also increased the absorption of sunlight by the active layer. Specifically, the work function of Ag is 4.26 eV, which has a large potential barrier with the HTL to induce energy loss. While when OLCNs modified the Ag, the work function increased to 4.40 eV, which could effectively reduce the energy loss (Figs. 8a and 8b). Meanwhile, the uniform distribution of OLCNs on the interfacial layer enhanced the optical electric field distribution (Figs. 8c and 8d), which improved the optical absorption of the active layer. In addition, OLCNs captured near-infrared light and transfer the photo-generated charges to the inherent interface traps at the interface of MoO$_3$ and OLCNs, which could overcome the high activation barrier of charges and the inherent defects of semiconductor oxide, and the schematic diagram was given in Fig. 8(e). Based on the combined effect of the above, both the interfacial charge transfer channel and the optical absorption were enhanced, which led to a significant improvement in the performance of OSCs.

Down conversion materials

CDs have great potential to be used as up/down-conversion materials for OSCs due to their Stokes and anti-Stokes shift properties, which can broaden the spectral absorption range of the active layer and further improve the device performance. It is well known that the insufficient utilization of sunlight is one of the primary reasons for the low efficiency of OSCs. CDs have strong absorption in the ultraviolet region, in which short-wavelength photons can converted to longer-wavelength photons, which are emitted in the visible region and absorbed by the active layer material. Therefore, CDs can also be as an ideal down-conversion material.

Cai et al.[90] prepared CQDs with down-conversion characteristics by microwave method with citric acid and urea as raw materials, and doped with P3HT:PC$_{61}$BM active layer to improve the device efficiency from 3.18% to 4.31%. Yang et al.[48] synthesized CQDs using glucose and 4,7,10-trioxy-1,13-tridecanediamino as raw materials by microwave method, and used them as the ETL to reduce the work function of ITO. At the same time, CQDs could convert near ultraviolet light to visible light with lower energy, which increased the optical absorption intensity of the active layer, and the device performance increased from 4.14% to 8.13%. Chen et al.[64] prepared the g-C$_3$N$_4$ with down-conversion performance (Fig. 9a), and prepared the OSCs with the device structure of ITO/ZnO/g-C$_3$N$_4$:active layer/PEDOT:PSS/MoO$_3$/Ag (Fig. 9b). From Figs. 9(c), 9(d) and 9(e), the EQE spectra, which were obtained by doping g-C$_3$N$_4$ into three different active layers (P3HT:PC$_{61}$BM, PBDTTT-C:PC$_{71}$BM, PTB7-Th:PC$_{71}$BM), respectively, showed that the introduction of g-C$_3$N$_4$ enhanced the photoelectric response intensity of the active layer material below 400 nm, thereby increasing the photocurrent as a
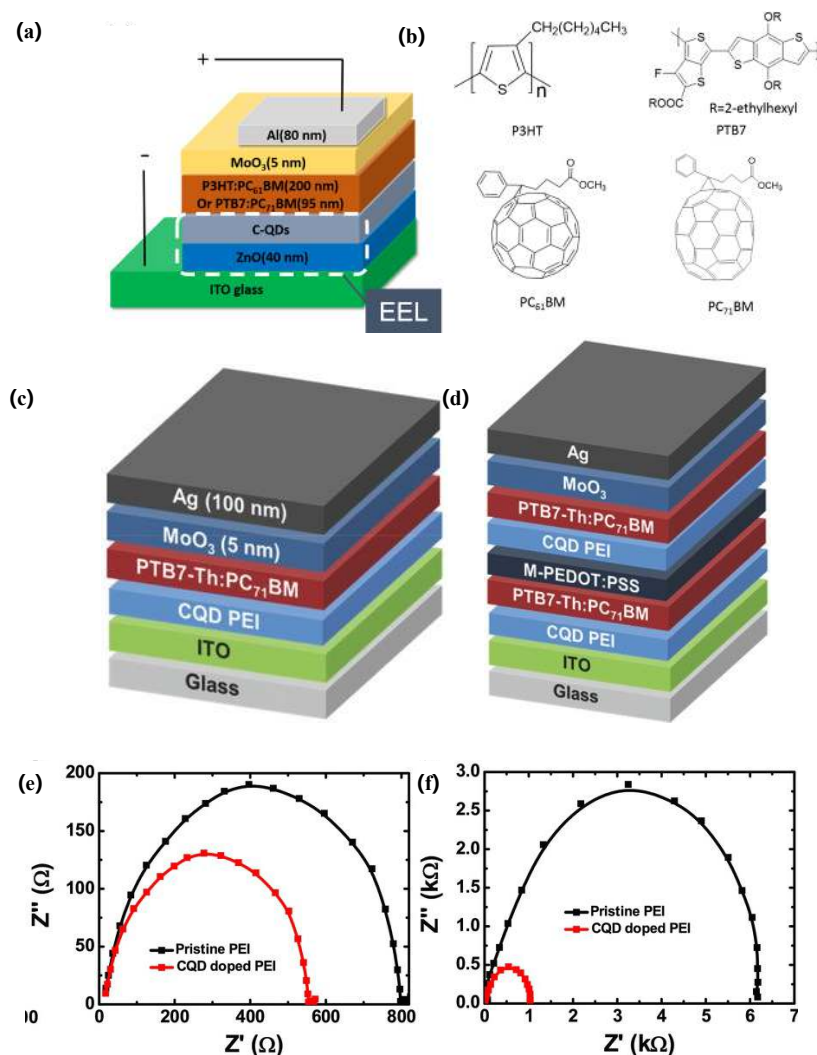
Fig. 7 (a) Device structure of inverted OSCs based on CQDs; (b) Molecular structures of P3HT, PTB7, PC$_{61}$BM and PC$_{71}$BM. (Reproduced with permission from Ref. [87]; Copyright (2018) American Chemical Society); Device structures of (c) single and (d) multi junction organic solar cell with CQDs doped PEI as the ETL; Impedance diagrams of (e) single and (f) multi junction organic solar cell. (Reproduced with permission from Ref. [88]; Copyright (2018) Wiley).

whole and effectively improving the device performance. In addition, Huang *et al.*[91] coated CQDs with down-conversion properties on ITO, which increased the absorption of active layer materials to the ultraviolet and blue light, and the efficiency increased by 12% compared with the reference device efficiency. However, there are few reports on the application of CDs as up-conversion materials in OSCs, which is worthy of further exploration.

SUMMARY AND OUTLOOK

CDs show a great application potential in the development of low-cost, high-efficiency and large-area printed OSCs due to their advantages of low toxicity, excellent photoelectric performance, excellent solution processing and up/down conversion. At present, CDs are mainly used as three materials in OSCs. (1) Active layer materials. Because CDs have broader

spectral absorption and matching energy level structure than fullerenes and their derivatives, their introduction into the active layer of OSCs is conducive to broadening the spectral absorption of the active layer and lowering the energy level barrier of the active layer, effectively enhancing the photoelectric conversion efficiency of OSCs. (2) Interface layer materials. Because of the tunable energy level structure, excellent solution processing performance and strong ultraviolet absorption capability of CDs, they can be used as electron/hole transport layer or interface modification layer, which can facilitate the adjustment of the energy level structure at the interface of the cell and reduce the energy loss of the device, and block the damage caused by ultraviolet light to the active layer materials to improve the stability of the cell. (3) Up/down conversion materials. The up/down conversion characteristics of CDs is favorable for broadening the spectral absorption range of OSCs to further enhance the performance,
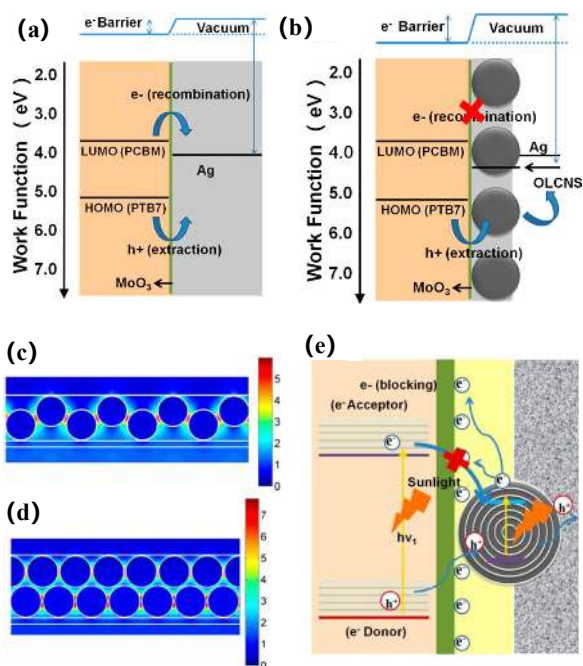
Fig. 8 The charge transfer process of device structure with (a) active layer/MoO$_3$/Ag and (b) active layer/MoO$_3$/OLCNs:Ag; the photoelectric field distribution of (c) a simple OLCNs layer and (d) OLCNs bilayers; (e) Charge transfer of electron acceptor, donor and OLCNs. (Reproduced with permission from Ref. [89]; Copyright (2017) American Chemical Society).

which is worthy of attention in a new application area of OSCs.

However, CDs still have obvious shortcomings when applied to OSCs: (1) The complex purification process and low yield limit the large-scale produce of CDs for the application in OSCs. (2) CDs with narrow absorption range and low absorbance limit their up/down conversion fluorescence capability, which has an influence on the performance of CDs based OSCs. (3) The mechanism of the physical-chemical, optical and electrical interactions between CDs and the functional layers of OSCs is not clear, which cannot effectively guide the preparation of high-performance CDs-based OSCs.

Aiming at the above-mentioned problems, researchers should pay more attention to the following investigation. On the one hand, establishing and improving the theoretical system to guide the controllable synthesis of CDs with excellent photoelectric properties and up/down conversion property, which can compensate for the deficiency of non-fullerene materials in OSCs that cannot fully utilize the solar spectrum, and enhance their performance to an advanced level. On the other hand, CDs should be widely used in various high-performance OSCs, and the interaction mechanism of the surface states of CDs and the functional layers of OSCs should be established through systematic investigation, so as to provide the experimental and theoretical guidance for improving the efficiency and stability of CDs-based OSCs.

In summary, CDs have a great potential for commercial application of OSCs as the interfacial layer and up/down conversion materials. Moreover, their advantages, including low cost, low toxicity and good solution processability, not only can facilitate the realization of the roll-to-roll printing of OSCs, but also effectively reduce their manufacturing costs. The continuous development of advanced high-performance CDs and CDs-based composite interface materials is of great significance to improve the photoelectric conversion efficiency and stability of OSCs. It is believed that CDs is worthy of further development and will play a greater role in the field of OSCs in future.
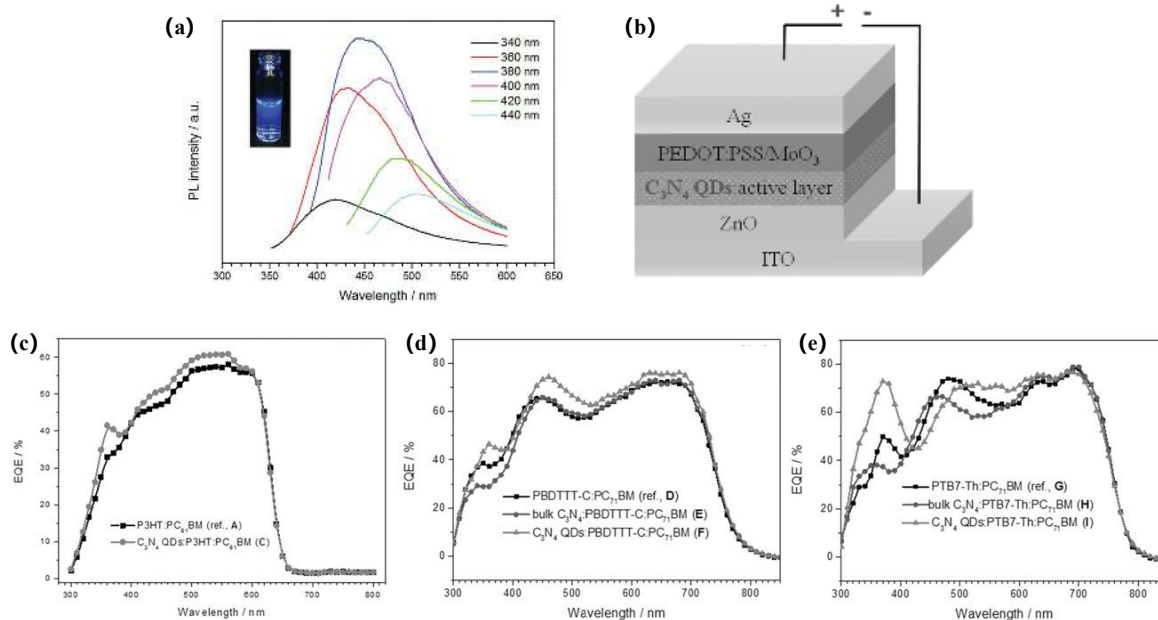

Fig. 9 (a) PL spectra of g-C$_3$N$_4$ under 340–440 nm excitation; (b) Device structure of organic solar cell doped with g-C$_3$N$_4$. The EQE spectra of OSCs based on (c) P3HT: PC$_{61}$BM, (d) PBDTTT-C:PC$_{71}$BM and (e) PTB7-Th:PC$_{71}$BM. (Reproduced with permission from Ref. [64]; Copyright (2016) Wiley).

BIOGRAPHY

Yong-Zhen Yang obtained her Ph.D. degree in materials science from Taiyuan University of Technology (TYUT) in 2007. Before that she was an engineer of Shanxi Coking Group Co., LTD. Since 2007, she joined TYUT and currently is a professor and doctoral supervisor of the Key Laboratory of Interface Science and Engineering in Advanced Materials in TYUT. From 2017 to 2018, she was as a visiting scholar in University of Hertfordshire, UK. She leads a group engaged in the synthesis of functionalized carbon nanomaterials and their applications in the field of optoelectronic and biomedicine.

Ling-Peng Yan received his Ph.D. degree in materials science and engineering from TYUT in 2017. After that he was appointed as a lecturer at TYUT. From 2019 to 2021, he did his postdoctoral research at Suzhou Institute of Nano-Tech and Nano-Bionics, Chinese Academy of Sciences (SINANO, CAS) with Prof. Chang-Qi Ma. He is now an associate researcher at TYUT. His research interests are focused on the stability of organic solar cells and synthesis and application of carbon nanomaterials.

Notes

The authors declare no competing financial interest.

ACKNOWLEDGMENTS

REFERENCES

1   Chatterjee, S.; Jinnai, S.; Ie, Y. Nonfullerene acceptors for P3HT-based organic solar cells. *J. Mater. Chem. A* **2021**.
2   Zhao, C. W.; Zhang, Z.; Han, F. M.; Xia, D. D.; Xiao, C. Y.; Fang, J.; Zhang, Y. F.; Wu, B. H.; You, S. Y.; Wu, Y. G.; Li, W. W. An organic-inorganic hybrid electrolyte as a cathode interlayer for efficient organic solar cells. *Angew. Chem. Int. Ed.* **2021**, *60*, 8526–8531.
3   Wang, G.; Melkonyan, F. S.; Facchetti, A.; Marks, T. J. All-polymer solar cells: Recent progress, challenges, and prospects. *Angew. Chem. Int. Ed.* **2019**, *58*, 4129–4142.
4   Cheng, P.; Zhan, X. W. Stability of organic solar cells: challenges and strategies. *Chem. Soc. Rev.* **2016**, *45*, 2544–2582.
5   Po, R.; Carbonera, C.; Bernardi, A.; Camaioni, N. The role of buffer layers in polymer solar cells. *Energ. Environ. Sci.* **2011**, *4*, 285–310.
6   Mirsafaei, M.; Fallahpour, A. H.; Lugli, P.; Rubahn, H. G.; Adam, J.; Madsen, M. The influence of electrical effects on device performance of organic solar cells with nano-structured electrodes. *Sci. Rep.* **2017**, *7*, 5300.
7   Yuan, J.; Zhang, Y. Q.; Zhou, L. Y.; Zhang, G. C.; Yip, H. L.; Lau, T. K.; Lu, X. H.; Zhu, C.; Peng, H. J.; Johnson, P. A.; Leclerc, M.; Cao, Y.; Ulanski, J.; Li, Y. F.; Zou, Y. P. Single-junction organic solar cell with over 15% efficiency using fused-ring acceptor with electron-deficient core. *Joule* **2019**, *3*, 1140–1151.
8   Hong, L.; Yao, H. F.; Wu, Z.; Cui, Y.; Zhang, T.; Xu, Y.; Yu, R. N.; Liao, Q.; Gao, B. W.; Xian, K. H.; Woo, H. Y.; Ge, Z. Y.; Hou, J. H. Eco-compatible solvent-processed organic photovoltaic cells with over 16% efficiency. *Adv. Mater.* **2019**, *31*, 1903441.
9   Zhu, F.; Chen, X. H.; Lu, Z.; Yang, J. X.; Huang, S. M.; Sun, Z. Efficiency enhancement of inverted polymer solar cells using ionic liquid-functionalized carbon nanoparticles-modified ZnO as electron selective layer. *Nano-Micro. Lett.* **2014**, *6*, 24–29.
10 Kim, J. K.; Park, M. J.; Kim, S. J.; Wang, D. H.; Cho, S. P.; Bae, S.; Park, J. H.; Hong, B. H. Balancing light absorptivity and carrier conductivity of graphene quantum dots for high-efficiency bulk heterojunction solar cells. *ACS Nano* **2013**, *7*, 7207–7212.
11 Dabera, G. D. M. R.; Jayawardena, K. D. G. I.; Prabhath, M. R. R.; Yahya, I.; Tan, Y. Y.; Nismy, N. A.; Shiozawa, H.; Sauer, M.; Ruiz-Soria, G.; Ayala, P.; Stolojan, V.; Adikaari, A. A. D. T.; Jarowski, P. D.; Pichler, T.; Silva, S. R. P. Hybrid carbon nanotube networks as efficient hole extraction layers for organic photovoltaics. *ACS Nano* **2013**, *7*, 556–565.
12 Mihailetchi, V. D.; Xie, H. X.; de Boer, B.; Koster, L. J. A.; Blom, P. W. M. Charge transport and photocurrent generation in poly(3-hexylthiophene): methanofullerene bulk-heterojunction solar cells. *Adv. Funct. Mater.* **2006**, *16*, 699–708.
13 Lee, Y. Y.; Tu, K. H.; Yu, C. C.; Li, S. S.; Hwang, J. Y.; Lin, C. C.; Chen, K. H.; Chen, L. C.; Chen, H. L.; Chen, C. W. Top laminated graphene electrode in a semitransparent polymer solar cell by simultaneous thermal annealing/releasing method. *ACS Nano* **2011**, *5*, 6564–6570.
14 Lee, J. M.; Kwon, B. H.; Park, H. I.; Kim, H.; Kim, M. G.; Park, J. S.; Kim, E. S.; Yoo, S.; Jeon, D. Y.; Kim, S. O. Exciton dissociation and charge-transport enhancement in organic solar cells with quantum-dot/N-doped CNT hybrid nanomaterials. *Adv. Mater.* **2013**, *25*, 2011–2017.
15 Lin, X. F.; Yang, Y. Z.; Nian, L.; Su, H.; Ou, J. M.; Yuan, Z. K.; Xie, F. Y.; Hong, W.; Yu, D. S.; Zhang, M. Q.; Ma, Y. G.; Chen, X. D. Interfacial modification layers based on carbon dots for efficient inverted polymer solar cells exceeding 10% power conversion efficiency. *Nano Energy* **2016**, *26*, 216–223.
16 Zheng, Z.; Awartani, O. M.; Gautam, B.; Liu, D. L.; Qin, Y. P.; Li, W. N.; Bataller, A.; Gundogdu, K.; Ade, H.; Hou, J. H. Efficient charge transfer and fine-tuned energy level alignment in a THF-processed fullerene- free organic solar cell with 11.3% efficiency. *Adv. Mater.* **2017**, *29*, 1604241.
17 Mishra, V.; Patil, A.; Thakur, S.; Kesharwani, P. Carbon dots: Emerging theranostic nanoarchitectures. *Drug. Discov. Today* **2018**, *23*, 1219–1232.
18 Cai, T. T.; Liu, B.; Pang, E. N.; Ren, W. J.; Li, S. J.; Hu, S. L. A review on the preparation and applications of coal-based fluorescent carbon dots. *New Carbon Materials* **2020**, *35*, 646–664.
19 Yue, L. J.; Wei, Y. Y.; Fan, J. B.; Chen, L.; Li, Q.; Du, J. L.; Yu, S. P.; Yang, Y. Z. Research progress in the use of cationic carbon dots for the integration of cancer diagnosis with gene treatment. *New Carbon Materials* **2021**, *36*, 373–389.
20 Cui, B.; Feng, X. T.; Zhang, F.; Wang, Y. L.; Liu, X. G.; Yang, Y. Z.; Jia, H. S. The use of carbon quantum dots as fluorescent materials in white LEDs. *New Carbon Materials* **2017**, *32*, 385–401.
21 Yang, S. T.; Cao, L.; Luo, P. G. J.; Lu, F. S.; Wang, X.; Wang, H. F.; Meziani, M. J.; Liu, Y. F.; Qi, G.; Sun, Y. P. Carbon dots for optical imaging *in vivo*. *J. Am. Chem. Soc.* **2009**, *131*, 11308–11309.
22 Xu, X.; Ray, R.; Gu, Y.; Ploehn, H. J.; Gearheart, L.; Raker, K.;

Scrivens, W. A. Electrophoretic analysis and purification of fluorescent single-walled carbon nanotube fragments. *J. Am. Chem. Soc.* **2015**, *126*, 12736–7.

23 Zhao, Q. L.; Zhang, Z. L.; Huang, B. H.; Peng, J.; Zhang, M.; Pang, D. W. Facile preparation of low cytotoxicity fluorescent carbon nanocrystals by electrooxidation of graphite. *Chem. Commun.* **2008**, 5116–5118.

24 Li, W. D.; Liu, Y.; Wang, B. Y.; Song, H. Q.; Liu, Z. Y.; Lu, S. Y.; Yang, B. Kilogram-scale synthesis of carbon quantum dots for hydrogen evolution, sensing and bioimaging. *Chinese Chem. Lett.* **2019**, *30*, 2323–2327.

25 Kang, C.; Huang, Y.; Yang, H.; Yan, X. F.; Chen, Z. P. A review of carbon dots produced from biomass wastes. *Nanomaterials-Basel.* **2020**, *10*, 2316.

26 Achilleos, D. S.; Yang, W. X.; Kasap, H.; Savateev, A.; Markushyna, Y.; Durrant, J. R.; Reisner, E. Solar reforming of biomass with homogeneous carbon dots. *Angew. Chem. Int. Ed.* **2020**, *59*, 18184–18188.

27 Zhu, S. J.; Meng, Q. N.; Wang, L.; Zhang, J. H.; Song, Y. B.; Jin, H.; Zhang, K.; Sun, H. C.; Wang, H. Y.; Yang, B. Highly photoluminescent carbon dots for multicolor patterning, sensors, and bioimaging. *Angew. Chem. Int. Ed.* **2013**, *52*, 3953–3957.

28 Tomskaya, A. E.; Egorova, M. N.; Kapitonov, A. N.; Nikolaev, D. V.; Popov, V. I.; Fedorov, A. L.; Smagulova, S. A. Synthesis of luminescent n-doped carbon dots by hydrothermal treatment. *Phys. Status. Solidi. B.* **2018**, *255*, 1700222.

29 Liu, Y.; Xiao, N.; Gong, N. Q.; Wang, H.; Shi, X.; Gu, W.; Ye, L. One-step microwave-assisted polyol synthesis of green luminescent carbon dots as optical nanoprobes. *Carbon* **2014**, *68*, 258–264.

30 Bourlinos, A. B.; Stassinopoulos, A.; Anglos, D.; Zboril, R.; Karakassides, M.; Giannelis, E. P. Surface functionalized carbogenic quantum dots. *Small* **2008**, *4*, 455–458.

31 Wang, B. Y.; Song, H. Q.; Qu, X. L.; Chang, J. B.; Yang, B.; Lu, S. Y. Carbon dots as a new class of nanomedicines: opportunities and challenges. *Coordin. Chem. Rev.* **2021**, *442*, 214010.

32 Guo, R. T.; Li, L.; Wang, B. W.; Xiang, Y. G.; Zou, G. Q.; Zhu, Y. R.; Hou, H. S.; Ji, X. B. Functionalized carbon dots for advanced batteries. *Energy Storage Mater.* **2021**, *37*, 8–39.

33 Rigodanza, F.; Burian, M.; Arcudi, F.; Dordevic, L.; Amenitsch, H.; Prato, M. Snapshots into carbon dots formation through a combined spectroscopic approach. *Nat. Commun.* **2021**, *12*, 2640.

34 Li, D.; Jing, P. T.; Sun, L. H.; An, Y.; Shan, X. Y.; Lu, X. H.; Zhou, D.; Han, D.; Shen, D. Z.; Zhai, Y. C.; Qu, S. N.; Zboril, R.; Rogach, A. L. Near-infrared excitation/emission and multiphoton-induced fluorescence of carbon dots. *Adv. Mater.* **2018**, *30*, 1705913.

35 Zhu, S. J.; Song, Y. B.; Zhao, X. H.; Shao, J. R.; Zhang, J. H.; Yang, B. The photoluminescence mechanism in carbon dots (graphene quantum dots, carbon nanodots, and polymer dots): Current state and future perspective. *Nano Res.* **2015**, *8*, 355–381.

36 Lv, K. L.; Suo, W. Q.; Shao, M. D.; Zhu, Y.; Wang, X. P.; Feng, J. J.; Fang, M. W. Nitrogen doped MoS_2 and nitrogen doped carbon dots composite catalyst for electroreduction CO_2 to CO with high faradaic efficiency. *Nano Energy* **2019**, *63*, 103834.

37 Song, H. Q.; Liu, X. J.; Wanga, B. Y.; Tang, Z. Y.; Lu, S. Y. High production-yield solid-state carbon dots with tunable photoluminescence for white/multi-color light-emitting diodes. *Sci. Bull.* **2019**, *64*, 1788–1794.

38 Hola, K.; Sudolska, M.; Kalytchuk, S.; Nachtigallova, D.; Rogach, A. L.; Otyepka, M.; Zboril, R. Graphitic nitrogen triggers red fluorescence in carbon dots. *ACS Nano* **2017**, *11*, 12402–12410.

39 Tang, L. B.; Ji, R. B.; Li, X. M.; Bai, G. X.; Liu, C. P.; Hao, J. H.; Lin, J. Y.; Jiang, H. X.; Teng, K. S.; Yang, Z. B.; Lau, S. P. Deep ultraviolet to near-infrared emission and photoresponse in layered N-doped graphene quantum dots. *ACS Nano* **2014**, *8*, 6312–6320.

40 Zheng, X. T.; Ananthanarayanan, A.; Luo, K. Q.; Chen, P. Glowing graphene quantum dots and carbon dots: Properties, syntheses, and biological applications. *Small* **2015**, *11*, 1620–1636.

41 Wu, Z. L.; Liu, Z. X.; Yuan, Y. H. Carbon dots: materials, synthesis, properties and approaches to long-wavelength and multicolor emission. *J. Mater. Chem. B* **2017**, *5*, 3794–3809.

42 Yeh, T. F.; Huang, W. L.; Chung, C. J.; Chiang, I. T.; Chen, L. C.; Chang, H. Y.; Su, W. C.; Cheng, C.; Chen, S. J.; Teng, H. S. Elucidating quantum confinement in graphene oxide dots based on excitation-wavelength-independent photoluminescence. *J. Phys. Chem. Lett.* **2016**, *7*, 2087–2092.

43 Bao, L.; Zhang, Z. L.; Tian, Z. Q.; Zhang, L.; Liu, C.; Lin, Y.; Qi, B. P.; Pang, D. W. Electrochemical tuning of luminescent carbon nanodots: from preparation to luminescence mechanism. *Adv. Mater.* **2011**, *23*, 5801–5806.

44 Su, Y.; Xie, Z. G.; Zheng, M. Carbon dots with concentration-modulated fluorescence: aggregation-induced multicolor emission. *J. Colloid. Interf. Sci.* **2020**, *573*, 241–249.

45 Li, H. T.; He, X. D.; Kang, Z. H.; Huang, H.; Liu, Y.; Liu, J. L.; Lian, S. Y.; Tsang, C. H. A.; Yang, X. B.; Lee, S. T. Water-soluble fluorescent carbon quantum dots and photocatalyst design. *Angew. Chem. Int. Edit.* **2010**, *49*, 4430–4434.

46 Tian, R. X.; Hu, S. L.; Wu, L. L.; Chang, Q.; Yang, J. L.; Liu, J. Tailoring surface groups of carbon quantum dots to improve photoluminescence behaviors. *Appl. Surf. Sci.* **2014**, *301*, 156–160.

47 Behera, R. K.; Sau, A.; Mishra, L.; Bera, K.; Mallik, S.; Nayak, A.; Basu, S.; Sarangi, M. K. Redox modifications of carbon dots shape their optoelectronics. *J. Phys. Chem. C.* **2019**, *123*, 27937–27944.

48 Yang, Y. Z.; Lin, X. F.; Li, W. L.; Ou, J. M.; Yuan, Z. K.; Xie, F. Y.; Hong, W.; Yu, D. S.; Ma, Y. G.; Chi, Z. G.; Chen, X. D. One-pot large-scale synthesis of carbon quantum dots: efficient cathode interlayers for polymer solar cells. *ACS Appl. Mater. Inter.* **2017**, *9*, 14953–14959.

49 Pan, L. L.; Sun, S.; Zhang, A. D.; Jiang, K.; Zhang, L.; Dong, C. Q.; Huang, Q.; Wu, A. G.; Lin, H. W. Truly fluorescent excitation-dependent carbon dots and their applications in multicolor cellular imaging and multidimensional sensing. *Adv. Mater.* **2015**, *27*, 7782–7787.

50 Fu, M.; Ehrat, F.; Wang, Y.; Milowska, K. Z.; Reckmeier, C.; Rogach, A. L.; Stolarczyk, J. K.; Urban, A. S.; Feldmann, J. Carbon dots: a unique fluorescent cocktail of polycyclic aromatic hydrocarbons. *Nano Lett.* **2015**, *15*, 6030–6035.

51 Zhan, J.; Geng, B. J.; Wu, K.; Xu, G.; Wang, L.; Guo, R. Y.; Lei, B.; Zheng, F. F.; Pan, D. Y.; Wu, M. H. A solvent-engineered molecule fusion strategy for rational synthesis of carbon quantum dots with multicolor bandgap fluorescence. *Carbon* **2018**, *130*, 153–163.

52 Lu, S. Y.; Sui, L. Z.; Liu, J. J.; Zhu, S. J.; Chen, A. M.; Jin, M. X.; Yang, B. Near-infrared photoluminescent polymer-carbon nanodots with two-photon fluorescence. *Adv. Mater.* **2017**, *29*, 1603443.

53 Zhang, M. L.; Hu, L. L.; Wang, H. B.; Song, Y. X.; Liu, Y.; Li, H.; Shao, M. W.; Huang, H.; Kang, Z. H. One-step hydrothermal synthesis of chiral carbon dots and their effects on mung bean plant growth.

Nanoscale **2018**, *10*, 12734–12742.

54 Jia, X. F.; Li, J.; Wang, E. K. One-pot green synthesis of optically pH-sensitive carbon dots with upconversion luminescence. *Nanoscale* **2012**, *4*, 5572–5575.

55 Shen, J. H.; Zhu, Y. H.; Chen, C.; Yang, X. L.; Li, C. Z. Facile preparation and upconversion luminescence of graphene quantum dots. *Chem. Commun.* **2011**, *47*, 2580–2582.

56 Lu, S. Y.; Yang, B. One step synthesis of efficient orange-red emissive polymer carbon nanodots displaying unexpect two photon fluorescence. *Acta Polymerica Sinica* (in Chinese) **2017**, 1200–1206.

57 Zhan, Q. Q.; Wang, B. J.; Wen, X. Y.; He, S. L. Controlling the excitation of upconverting luminescence for biomedical theranostics: neodymium sensitizing. *Opt. Mater. Express* **2016**, *6*, 1011–1023.

58 Molaei, M. J. The optical properties and solar energy conversion applications of carbon quantum dots: a review. *Sol. Energy* **2020**, *196*, 549–566.

59 He, C.; Peng, L. K.; Lv, L. Z.; Cao, Y.; Tu, J. C.; Huang, W.; Zhang, K. X. *In situ* growth of carbon dots on TiO_2 nanotube arrays for PEC enzyme biosensors with visible light response. *RSC Adv.* **2019**, *9*, 15084–15091.

60 Lee, E.; Ryu, J.; Jang, J. Fabrication of graphene quantum dots *via* size-selective precipitation and their application in upconversion-based dsscs. *Chem. Commun.* **2013**, *49*, 9995–9997.

61 Zhu, S. J.; Zhang, J. H.; Liu, X.; Li, B.; Wang, X. F.; Tang, S. J.; Meng, Q. N.; Li, Y. F.; Shi, C.; Hu, R.; Yang, B. Graphene quantum dots with controllable surface oxidation, tunable fluorescence and up-conversion emission. *RSC Adv.* **2012**, *2*, 2717–2720.

62 Shockley, W.; Queisser, H. J. Detailed balance limit of efficiency of *p-n* junction solar cells. *J. Appl. Phys.* **1961**, *32*, 510–519.

63 Richards, B. S. Enhancing the performance of silicon solar cells *via* the application of passive luminescence conversion layers. *Sol. Energ. Mat. Sol. C.* **2006**, *90*, 2329–2337.

64 Chen, X.; Liu, Q.; Wu, Q. L.; Du, P. W.; Zhu, J.; Dai, S. Y.; Yang, S. F. Incorporating graphitic carbon nitride (g-C_3N_4) quantum dots into bulk-heterojunction polymer solar cells leads to efficiency enhancement. *Adv. Funct. Mater.* **2016**, *26*, 1719–1728.

65 Liu, Q.; Jiang, Y.; Jin, K.; Qin, J.; Ding, L. 18% Efficiency organic solar cells. *Sci. Bull.* **2020**, *65*, 272–275.

66 Zhang, Q. Q. The preparation and application of carbon dots composites, Master's thesis, Beijing University of Chemical Technology, 2018.

67 Liu, X. H. Study on the fabrication and perfoemance of organic solar cells based on the modified ZnO interlayer, Doctoral Dissertation, Chinese Academy of Sciences, 2017.

68 Angelini, G.; De Maria, P.; Fontana, A.; Pierini, M.; Maggini, M.; Gasparrini, F.; Zappia, G. Study of the aggregation properties of a novel amphiphilic C_{60} fullerene derivative. *Langmuir* **2001**, *17*, 6404–6407.

69 Kwon, W.; Lee, G.; Do, S.; Joo, T.; Rhee, S. W. Size-controlled soft-template synthesis of carbon nanodots toward versatile photoactive materials. *Small* **2014**, *10*, 506–513.

70 Sharma, R.; Alam, F.; Sharma, A. K.; Dutta, V.; Dhawan, S. K. Role of zinc oxide and carbonaceous nanomaterials in non-fullerene-based polymer bulk heterojunction solar cells for improved cost-to-performance ratio. *J. Mater. Chem. A* **2015**, *3*, 22227–22238.

71 Lim, H.; Lee, K. S.; Liu, Y.; Kim, H. Y.; Son, D. I. Photovoltaic performance of inverted polymer solar cells using hybrid carbon quantum dots and absorption polymer materials. *Electron Mater. Lett.* **2018**, *14*, 581–586.

72 Liu, C. Y.; Chang, K. W.; Guo, W. B.; Li, H.; Shen, L.; Chen, W. Y.; Yan, D. W. Improving charge transport property and energy transfer with carbon quantum dots in inverted polymer solar cells. *Appl. Phys. Lett.* **2014**, 105.

73 Zhang, X. Y.; Li, Z. Q.; Zhang, Z. H.; Liu, C. Y.; Li, J. F.; Guo, W. B.; Qu, S. N. Employing easily prepared carbon nanoparticles to improve performance of inverted organic solar cells. *ACS Sustain Chem. Eng.* **2016**, *4*, 2359–2365.

74 Cui, B.; Yan, L. P.; Gu, H. M.; Yang, Y. Z.; Liu, X. G.; Ma, C. Q.; Chen, Y. K.; Jia, H. S. Fluorescent carbon quantum dots synthesized by chemical vapor deposition: An alternative candidate for electron acceptor in polymer solar cells. *Opt. Mater.* **2018**, *75*, 166–173.

75 Wang, Y. W.; Lan, W. X.; Li, N.; Lan, Z. J.; Li, Z.; Jia, J. N.; Zhu, F. R. Stability of nonfullerene organic solar cells: From built-in potential and interfacial passivation perspectives. *Adv. Energy Mater.* **2019**, *9*, 1900157.

76 Wang, Y. L.; Yan, L. P.; Ji, G. Q.; Wang, C.; Gu, H. M.; Luo, Q.; Chen, Q.; Chen, L. W.; Yang, Y. Z.; Ma, C. Q.; Liu, X. G. Synthesis of N, S-doped carbon quantum dots for use in organic solar cells as the ZnO modifier to eliminate the light-soaking effect. *ACS Appl. Mater. Inter.* **2019**, *11*, 2243–2253.

77 Xu, H.; Zhang, L.; Ding, Z. C.; Hu, J. L.; Liu, J.; Liu, Y. C. Edge-functionalized graphene quantum dots as a thickness-insensitive cathode interlayer for polymer solar cells. *Nano Res.* **2018**, *11*, 4293–4301.

78 Ding, Z. C.; Miao, Z. S.; Xie, Z. Y.; Liu, J. Functionalized graphene quantum dots as a novel cathode interlayer of polymer solar cells. *J. Mater. Chem. A* **2016**, *4*, 2413–2418.

79 Yan, L. P.; Yang, Y. Z.; Ma, C. Q.; Liu, X. G.; Wang, H.; Xu, B. S. Synthesis of carbon quantum dots by chemical vapor deposition approach for use in polymer solar cell as the electrode buffer layer. *Carbon* **2016**, *109*, 598–607.

80 Li, M. M.; Ni, W.; Kan, B.; Wan, X. J.; Zhang, L.; Zhang, Q.; Long, G. K.; Zuo, Y.; Chen, Y. S. Graphene quantum dots as the hole transport layer material for high-performance organic solar cells. *Phys. Chem. Chem. Phys.* **2013**, *15*, 18973–18978.

81 Ding, Z. C.; Hao, Z.; Meng, B.; Xie, Z. Y.; Liu, J.; Dai, L. M. Few-layered graphene quantum dots as efficient hole-extraction layer for high-performance polymer solar cells. *Nano Energy.* **2015**, *15*, 186–192.

82 Zhang, H. J.; Zhang, Q.; Li, M. M.; Kan, B.; Ni, W.; Wang, Y. C.; Yang, X.; Du, C. X.; Wan, X. J.; Chen, Y. S. Investigation of the enhanced performance and lifetime of organic solar cells using solution-processed carbon dots as the electron transport layers. *J. Mater. Chem. C* **2015**, *3*, 12403–12409.

83 Hasani, A.; Gavgani, J. N.; Pashaki, R. M.; Baseghi, S.; Salehi, A.; Heo, D.; Kim, S. Y.; Mahyari, M. Poly(3,4 ethylenedioxythiophene):poly(styrenesulfonate)llron(III) porphyrin supported on S and N co-doped graphene quantum dots as a hole transport layer in polymer solar cells. *Sci. Adv. Mater.* **2017**, *9*, 1616–1625.

84 Kim, J. K.; Kim, S. J.; Park, M. J.; Bae, S.; Cho, S. P.; Du, Q. G.; Wang, D. H.; Park, J. H.; Hong, B. H. Surface-engineered graphene quantum dots incorporated into polymer layers for high performance organic photovoltaics. *Sci. Rep.* **2015**, *5*, 14276.

85 Dang, Y.; Wang, Y. H.; Shen, S.; Huang, S.; Qu, X. W.; Pang, Y.; Silva, S. R. P.; Kang, B. N.; Lu, G. Y. Solution processed hybrid graphene-MoO_3 hole transport layers for improved performance of organic

solar cells. *Org. Electron* **2019**, *67*, 95−100.

86 Zhao, W. S.; Yan, L. P.; Gu, H. M.; Li, Z. R.; Wang, Y. L.; Luo, Q.; Yang, Y. Z.; Liu, X. G.; Wang, H.; Ma, C. Q. Zinc oxide coated carbon dot nanoparticles as electron transport layer for inverted polymer solar cells. *ACS Appl. Energ. Mater.* **2020**, *3*, 11388−11397.

87 Zhang, R. Q.; Zhao, M.; Wang, Z. Q.; Wang, Z. T.; Zhao, B.; Miao, Y. Q.; Zhou, Y. J.; Wang, H.; Hao, Y. Y.; Chen, G.; Zhu, F. R. Solution-processable ZnO/carbon quantum dots electron extraction layer for highly efficient polymer solar cells. *ACS Appl. Mater. Inter.* **2018**, *10*, 4895−4903.

88 Kang, R.; Park, S.; Jung, Y. K.; Lim, D. C.; Cha, M. J.; Seo, J. H.; Cho, S. High-efficiency polymer homo-tandem solar cells with carbon quantum-dot-doped tunnel junction intermediate layer. *Adv. Energy. Mater.* **2018**, *8*, 1702165.

89 Li, Z. Q.; Dong, J. J.; Liu, C. Y.; Zhang, X. L.; Zhang, X. Y.; Shen, L.; Guo, W. B.; Zhang, L.; Long, Y. B. Improved optical field distribution and charge extraction through an interlayer of carbon nanospheres in polymer solar cells. *Chem. Mater.* **2017**, *29*, 2961−2968.

90 Wang, J. A.; Li, H. R.; Lei, Q.; Chang, F. Z.; Fan, W. H.; Zhang, H.; Cai, L. N. Dual-interface modification effect of carbon quantum dots on the performance of polymer solar cells. *J. Mater. Sci-Mater. El.*

2019, *30*, 11063−11069.

91 Huang, J. J.; Zhong, Z. F.; Rong, M. Z.; Zhou, X.; Chen, X. D.; Zhang, M. Q. An easy approach of preparing strongly luminescent carbon dots and their polymer based composites for enhancing solar cell efficiency. *Carbon* **2014**, *70*, 190−198.

92 Li, Z. Q.; Zhang, X. Y.; Liu, C. Y.; Guo, J. X.; Cui, H. X.; Shen, L.; Guo, W. B. Toward efficient carbon-dots-based electron-extraction layer through surface charge engineering. *ACS Appl. Mater. Interfaces* **2018**, *10*, 40255−40264.

93 Wang, S. C.; Li, Z. J.; Xu, X. P.; Zhang, G. J.; Li, Y.; Peng, Q. Amino-functionalized graphene quantum dots as cathode interlayer for efficient organic solar cells: quantum dot size on interfacial modification ability and photovoltaic performance. *Adv. Mater. Interfaces* **2019**, *6*, 1801480.

94 Juang, T. Y.; Kao, J. C.; Wang, J. C.; Hsu, S. Y.; Chen, C. P. Carbonized bamboo-derived carbon nanodots as efficient cathode interfacial layers in high-performance organic photovoltaics. *Adv. Mater. Interfaces* **2018**, *5*, 1800031.

95 Zhang, X. Y.; Liu, C. Y.; Li, Z. Q.; Guo, J. X.; Shen, L.; Guo, W. B.; Zhang, L.; Ruan, S. P.; Long, Y. B. An easily prepared carbon quantum dots and employment for inverted organic photovoltaic devices. *Chem. Eng. J.* **2017**, *315*, 621−629.